



A comprehensive methodological framework for 3D head anthropometric shape modeling of a small dataset

Leonardo H. Wei, S. Sudeesh, Sajal Chakroborty & Suman K. Chowdhury

To cite this article: Leonardo H. Wei, S. Sudeesh, Sajal Chakroborty & Suman K. Chowdhury (18 Jun 2025): A comprehensive methodological framework for 3D head anthropometric shape modeling of a small dataset, Ergonomics, DOI: [10.1080/00140139.2025.2518306](https://doi.org/10.1080/00140139.2025.2518306)

To link to this article: <https://doi.org/10.1080/00140139.2025.2518306>



[View supplementary material](#)



Published online: 18 Jun 2025.



[Submit your article to this journal](#)



Article views: 139



[View related articles](#)



[View Crossmark data](#)



A comprehensive methodological framework for 3D head anthropometric shape modeling of a small dataset

Leonardo H. Wei^a, S. Sudeesh^b , Sajal Chakraborty^c and Suman K. Chowdhury^d 

^aIndustrial, Manufacturing, and Systems Engineering, Texas Tech University, Lubbock, USA; ^bDepartment of Physical Medicine and Rehabilitation, Feinberg School of Medicine, Northwestern University, Chicago, IL, USA; ^cDepartment of Mathematical Sciences, Worcester Polytechnic Institute, Worcester, Massachusetts, USA; ^dIndustrial and Systems Engineering, University of Florida, Gainesville, USA

ABSTRACT

Efficient data analytics methods are essential to characterise occupation-specific anthropometric head shapes for developing well-fitted head-mounted devices. However, classifying and modelling 3D head shapes for small population groups remains challenging due to limited data and systematic approaches. This study proposes a streamlined six-step framework using 3D head scans from 36 firefighters (18 males, 18 females). We evaluated K-means and K-medoids clustering and four shape modelling methods—NURBS, NURBS least squares (LS), Cubic Spline, and Cubic Spline LS—and validated the predicted head shape against NIOSH, ANSUR II, CAESAR, and US Army databases. Results showed K-means outperformed K-medoids (28% lower distances). Surface mapping-based clustering was 35% more accurate than PCA-based clustering. Cubic Spline LS achieved the lowest mean squared error (0.70cm^2) and fastest computation (0.14s), performing better than NURBS LS (7.19cm^2 and 1.87 s). Overall, surface mapping, K-means clustering, and Cubic Spline LS methods provided more accurate head shapes for our study population groups.

Practitioner Summary: The proposed surface mapping-based K-means clustering and Cubic Spline LS method were efficient in predicting head shapes for specialised occupational groups. These techniques can assist practitioners for characterising and establishing occupation-specific anthropometric head shapes in order to develop well-fitted head-mounted devices (e.g., helmets, virtual reality headsets).

ARTICLE HISTORY

Received 17 April 2025
Accepted 3 June 2025

KEYWORDS

Small sample; NURBS; cubic spline; clustering; surface mapping; head 3D shape modelling

1. Introduction

Population-specific anthropometric head shape data are essential for designing well-fitted head-mounted products (e.g., helmets, virtual/augmented reality, headgear, headphones, etc.) (Niu and Li 2012; Ma and Niu 2021; Zhang et al. 2022b) and for creating head-neck finite element models (Bruneau and Cronin 2020), implants (Sena and Piyasin 2008; Mandolini et al. 2020), and their surgical planning (Dong et al. 2010; Rodriguez-Florez et al. 2017). Traditionally, one-dimensional (1D) measurements (e.g., head breadth, length, circumference, etc.)—obtained using rulers, tape measures, and anthropometers (Wang et al. 2000)—have been widely used to develop head anthropometry datasets because of their ease of data collection and processing. However, these manual measurements can be time-consuming and prone to error when untrained personnel or uncalibrated

equipment are involved. In contrast, the advancement in three-dimensional (3D) scanning technologies has garnered much attention in the past two decades, as 3D body scanners can capture intricate geometrical variations of human body shapes with high accuracy (Boehnen and Flynn 2005), which eventually yielded the development of new anthropometric head-shape datasets in several countries (Bougourd, Treleaven, and Allen 2004; Isaacs 2005; Seidl et al. 2009).

Although 3D scanners are faster, less labour-intensive, and incomparably more accurate and detailed than traditional 1D anthropometric measures, they produce a vast amount of 3D point clouds with complex geometries, curves, and contours. Furthermore, in comparison to 1D-based measures, 3D scan datasets require additional data analytics methods and steps for surface alignment, parameterisation, and dimensionality reduction before being used for body shape modelling

(Ma and Niu 2021). Such data processing steps are primarily attributed to between-subject variations in sitting behaviour, cervical lordotic curvatures, and the challenges in maintaining the same reference coordinate system between subjects during the scanning process. To mediate these challenges, previous studies suggested several techniques to align all acquired 3D scan data in the same reference plane or coordinate system. Some of these techniques include iterative closest point method (Luximon et al. 2016), the selection of facial landmark references (Zhuang et al. 2013), and alignment of model anatomical planes with global reference planes (Luximon, Ball, et al. 2012; Perret-Ellena et al. 2015; Skals et al. 2016). Additionally, since 3D shapes contain a massive number of dense point clouds, some previous studies have implemented principal component analysis (PCA), a dimensionality reduction technique, to reduce data dimensionality and to select major features that are significantly different from each other while protecting the original shape. However, no previous studies have tested whether the reduced dimension using PCA can represent complex 3D head shapes that differ significantly across subjects. Another alternative solution could be the development of a *surface mapping* method to represent the 3D complex head shape accurately while reducing the high dimensionality of its 3D point clouds. In other words, one can implement an effective surface mapping method that involves down-sampling of vast 3D point clouds while preserving the integrity of essential geometric features. Overall, all these intermediate steps collectively make the 3D shape-based head modelling more method-intensive than 1D-based methods.

The complexity of 3D head shape modelling is further compounded by wide variations in head shape between subjects, which can be attributed to factors such as age, gender, and ethnicity (Zhuang et al. 2013; Zhang et al. 2022a). As a result, large datasets have been utilised to develop various population-specific anthropometric head shapes. In those studies, unsupervised machine learning techniques such as K-medoid (Lacko et al. 2017; Verwulgen et al. 2018; Huang et al. 2023), hierarchical clustering (Skals et al. 2016; Ellena et al. 2017, 2018), and K-means (Niu, Li, and Salvendy 2009; Kuo, Wang, and Lu 2020; Seo, Kim, and Kim 2020) were commonly used to cluster the head shapes. Among them, contradictory results were reported in the utility of K-means and K-medoids in 3D shape clustering. For instance, Lacko et al. (2017) extracted two variations of features—1D measure and shape-based measures—from 100 head scans prior to implementing K-medoids technique. They found three

optimal clusters using the shape-based K-medoid method to yield the least amount of errors. Huang et al. (2023) also employed the K-medoids method to cluster 339 Chinese head scan data, yielding seven optimal clusters. Similarly, Niu, Li, and Salvendy (2009) employed the K-means algorithm to cluster 378 head scans of Chinese military personnel and reported obtaining seven distinct clusters. In another interesting study, Zhang et al. (2022c) employed K-means, hierarchical, and fuzzy clustering techniques on the principal components of the head scan point clouds and reported that six clusters yielded by the K-means method provided higher accuracy than other clustering techniques. In summary, there is no consensus on the accuracy and utility of K-means and K-medoid methods or the number of optimal clusters. The choice between them remains occupation- and population-specific (Niu, Li, and Salvendy 2009). Besides, techniques such as Ray-Turi index (Ray and Turi 1999), silhouette coefficient (Rousseeuw 1987), and elbow method (Nainggolan et al. 2019) were developed to determine the optimal number of clusters, though these methods do not provide any statistical significance when selecting the optimal number of clusters.

Data outliers can affect the performance of the clustering techniques. Though a large dataset may provide sufficient freedom to remove outliers, there exists very limited freedom for outlier removal with small datasets, as it may introduce data skewness and provide inappropriate shapes (Osborne and Overbay 2004). Although statistical shape modelling (Lacko et al. 2015; Heutinck et al. 2021; Zhang et al. 2022b; Fu, Luximon, and Luximon 2024; Liu et al. 2025) can mitigate some of these limitations; however, it typically demands large datasets, which are often infeasible in small, academic laboratories due to financial constraints and logistical burdens, particularly in acquiring 3D head scans from specialised occupational populations that do not exist locally in large numbers. Consequently, researchers need to identify appropriate clustering and head shape modelling techniques for small datasets to ensure the accuracy of the predicted shape and obtain meaningful results. Traditionally, researchers have commonly used curve fitting techniques, such as non-uniform rational B-splines (NURBS) (Piegl and Tiller 1997), Cubic Splines (Amor et al. 2006), linear regression (Weisberg 2005), and polynomial regression (Ostertagová 2012) to fit data points. However, for shape modelling and design, Cubic Splines and B-splines are the most used methods in modelling complex shapes due to their versatility in adjusting and modifying the curvature of shapes. In most cases, 3D curves and surface fitting begin with

parameterising the surface, essentially mapping its complex shape onto a simpler 2D space. This step plays a key role in making the fitting process more manageable. It not only helps achieve a smoother and more accurate fit but also improves computational efficiency. This step is especially important for methods like NURBS and cubic splines, which rely on a large number of parameters to define surface shape. The NURBS method provides local control over the shape of the curve through control points, allowing for localised modifications without substantially affecting the global curve shape. In contrast, the cubic spline method is defined by knot points that control the curvature of the shape. However, these knot points of the cubic spline do not provide as much flexibility as the control points in the NURBS technique in creating curvature, though they are simpler to implement and require less computational power. Additionally, researchers can choose *interpolation* or *approximation* functions when implementing NURBS and cubic spline methods to a given set of 3D data points (Piegl and Tiller 1997). While the *interpolation* function passes exactly through all data points, the *approximation* function does not necessarily pass through all data points. Instead, it minimises overall error (least squares error) between the function and the data points. In summary, for shape editing and customisation (i.e., adjustable sizes) using small 3D head scan dataset, a combination of NURBS or Cubic Spline method with an interpolation or approximation function would allow users to develop complex anthropometric head shapes in order to designing products that meet individual anthropometric needs (Zhang and Molenbroek 2004; Pal and Ballav 2007; Xie, Li, and Lv 2010; Hadi and Alias 2019; Xi, Zongqian, and Qiao 2022).

Although automatically adjustable products offer individualised fits, they have drawbacks, including being structurally less rigid, being more expensive, and requiring longer fabrication time. In contrast, products with fixed, variable sizes can become an inevitable option to facilitate a better fit, especially in the context of occupational products such as helmets. Nonetheless, a product developed using a civilian anthropometric dataset may not provide effective fit for occupation-specific populations, such as firefighters, law enforcement officers, and soldiers, who require unique anthropometric characteristics to meet their job-specific physical demands (Hsiao, Whisler, and Bradtmiller 2023). Additionally, the majority of these 3D anthropometric databases include 1-D measures and are based on civilian populations, like the Civilian American and European Surface Anthropometry Resource (CAESAR) (Robinette et al. 2002), National

Institute of Occupational Safety and Health (Zhuang and Bradtmiller 2005), size China (Ball 2011), and Taiwanese population (Wang, Wang, and Lin 2002). Moreover, these databases were developed decades ago and may no longer be adequate for developing head-mounted devices for the new generations due to changes in their anthropometric characteristics (Malkoc et al. 2014; Molenbroek, Albin, and Vink 2017). Lastly, literature shows the lack of digital head shapes that can readily be available to develop head-mounted devices such as 3D head shapes. These shortfalls indicate a critical need for an updated 3D head shape dataset, particularly for designing head protective devices used for both civilian and occupational users.

Therefore, this study aimed to determine accurate and efficient methods for clustering and modelling anthropometric head shapes using a small dataset. We conjecture that *NURBS* and *Cubic Spline* shape modelling techniques, when applied judiciously with appropriate clustering techniques, could reduce the effects of outliers and improve shape prediction even with a small dataset. To our knowledge, no studies have yet utilised these shape modelling methods in conjunction with K-means and/or K-medoid clustering techniques to derive anthropometrically-accurate 3D head shapes. In these contexts, this study introduced several methodological innovations: (1) develop a head surface mapping method inspired by the 10-20 system guidelines for electroencephalography data acquisition, (2) employ K-means and K-medoid clustering methods to the mapped surface and its reduced dimensional space to identify the most accurate clustering technique for small datasets, (3) propose an ANOVA-based strategy for identifying the optimal number of clusters, (4) employ both interpolation and approximation based NURBS and cubic spline curve fitting techniques to generate cluster-specific head shapes, and 5) derive 3D anthropometric digital head shapes for designing head-mounted product designs.

2. Materials and methods

2.1. Experiment

2.1.1. Participants

We initially recruited 36 firefighters, comprising 18 males and 18 females. However, the 3D scan data from seven female participants were excluded due to pre-processing challenges associated with ponytails and uneven hair volume. An additional seven male participants were recruited to ensure the acquisition of high-quality 3D scan data with minimal or no hair interference. This adjustment resulted in a final

participant cohort of 25 males (age: 37.6 ± 8.28 years; weight: 90 ± 17.17 kg; height: 177 ± 7 cm; BMI: 28.72 ± 4.58) and 11 females (age: 31.28 ± 7.17 years; weight: 63.11 ± 8.27 kg; height: 162 ± 5 cm; BMI: 24.28 ± 3.82). The inclusion criteria required all participants to be free from musculoskeletal, degenerative, or neurological disorders. Eligible participants were provided with detailed information about the study and were required to read and sign a consent form approved by the local Institutional Review Board (IRB No. 2020-708).

2.1.2. Data acquisition

A laser-based handheld 3D scanner (EinScan HX, Shining 3D, Hangzhou, China), equipped with two cameras, achieved an accuracy of 0.04 mm and a scanning speed of 50 fps, was used to scan participants' head and neck complex (from the T4 vertebral level to the tip of the head) in a controlled laboratory environment. To minimise interference from hair volume, all participants were asked to wear a swimming cap; female participants were specifically instructed to secure their ponytails beneath the cap. These head caps were carefully chosen to fit tightly against the scalp, with the purpose of creating indentations that reveal the underlying skull contour. That means the acquired scan data should accurately represent the true geometric contour of the 3D head shape, which can be used in the ergonomic design of head-mounted devices, such as helmets.

Additionally, participants were asked to maintain an upright seated posture with their eyes closed during the scanning process to ensure consistent and accurate data acquisition. To avoid any disruption to the laser scan, participants were instructed to remove metallic or reflective materials, such as jewellery. The scanning protocol was part of a larger project that involved three different scan conditions: no helmet, European-style helmet, and traditional US-style helmet. Each scanning session took approximately five minutes, resulting in a total scanning duration of 15 minutes per participant. However, for the purposes of anthropometric analysis, only the scans obtained without helmets were utilised.

2.2. Methodological framework for 3D head shape modelling

In order to sample and model 3D head scan data from a relatively small participant pool, we propose a methodological framework (Figure 1) consisting of six major steps: 1) data pre-processing, 2) surface mapping, 3) feature selection, 4) clustering, 5) shape modelling and

prediction, and 6) shape validation. In the subsequent sections, we demonstrate the intricate details of these steps.

Our data pre-processing steps included 1) noise, artefacts, and unwanted body feature removal, 2) 3D surface alignment, 3) data smoothing, and 4) head region of interest (ROI) selection. As raw 3D scan data contains noises and unwanted surface details (outliers), we used EXScan HX-V1.3.0.3 (Shining 3D, Hangzhou, China) software platform to remove noises, unwanted body segments (shoulder, upper back, and sternum regions) and other artefacts, such as clothes from the 3D raw scan data (Figure 1). As no consistent reference axis was maintained during the 3D scanning process across the subjects, all scan data must be aligned on a consistent axis for downstream processing. We used the digital NIOSH large head form as a baseline head shape (NIOSH 2020) and nine anthropometric landmarks (tip of the nose, right eye, left eye, mid-mouth, glabella, right ear opening, left ear opening, right nostril, and left nostril) to align 3D head shapes of all subjects to a reference axis (NIOSH). We used Geomagic Essentials software (Shining 3D, Hangzhou, China) to perform an automatic global registration process. By considering the nine landmarks as constraints, we aligned all scanned head shapes with the baseline reference head shape. We utilised an in-built smoothing function in Geomagic to smooth the 3D shape data and then cropped out unwanted neck, face, and skull segments to create the 3D head skull/scalp region of interest (ROI) for head shape clustering and modelling. The ROI was selected by intersecting three planes: a transverse plane passing through the glabella height, a sagittal plane passing through the tragion, and another transverse plane passing through the C1 height. The ROI comprised the upper region area resulting from the overlapping zones formed by the intersection of these planes (Figure 1).

2.2.1. Surface mapping

In this study, the proposed surface mapping process consisted of down-sampling the vast amount of 3D data points while preserving the essential geometric features of the head. Briefly, each shape (the ROI) was first aligned to three reference planes: mid-sagittal plane, mid-frontal plane, and Frankfurt plane passing through glabella and inion landmarks. Since each shape contained a vast amount of 3D point clouds (over 1 million data points), we applied a unique data reduction technique to streamline the process of clustering and modelling. Specifically, we created 18 equally spaced head curves along the anterior-posterior (A-P)

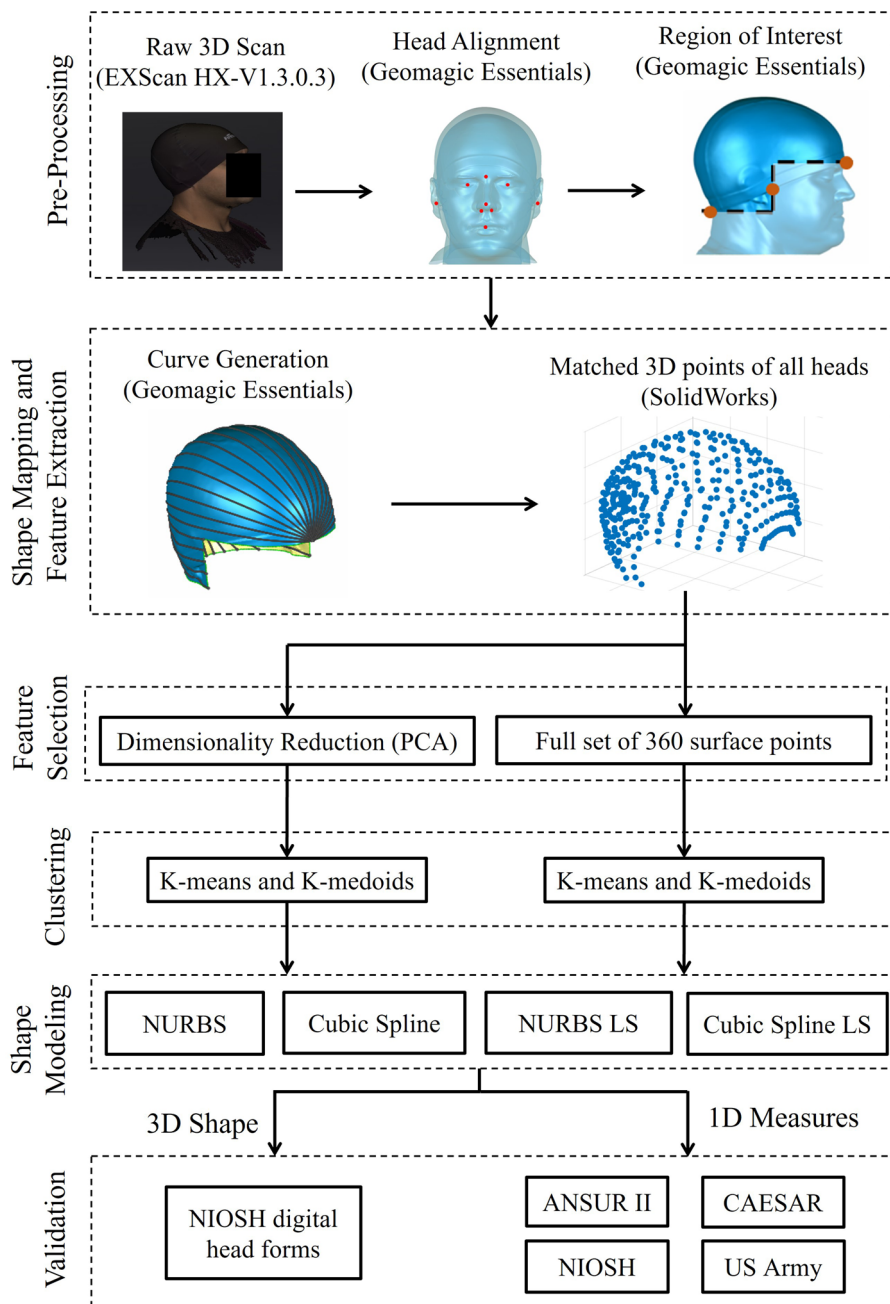


Figure 1. Methodological framework implemented in this study: 1) data pre-processing, 2) surface mapping, 3) feature selection, 4) clustering, 5) shape modelling and prediction, and 6) shape validation. Clustering methods were employed to both mapped surface and the principal components. Four shape modelling methods are non-uniform rational B-splines (NURBS), NURBS least squares (LS) approximation, Cubic Spline and Cubic Spline LS. Four anthropometric databases for validating the predicted shapes are NIOSH, ANSUR II, CAESAR, and US Army databases.

direction for each individual head shape (Figure 1). These curves were generated by first defining the Frankfurt plane and then rotating it around an axis passing through the glabella and occiput landmarks. The rotation was performed in 10° increments, starting from the left tragiion (0°) and ending at the right tragiion (180°). Along each of the 18 curves, we extracted 20 equally spaced points in the A-P direction using Geomagic software. This surface mapping process was inspired by the International 10-20 system guideline for

electroencephalography electrode placement (Jasper 1958). Our first set of clustering features consisted of a total of 360 surface points (18 curves × 20 equally spaced points per curve) for each individual subject.

2.2.2. Dimensionality reduction

To identify the most significant features and enhance clustering accuracy (Luximon, Zhang, et al. 2012), the PCA technique was applied to the magnitudes

(Euclidean norms) of the 360 surface points of the mapped surface across all subjects. The number of principal components (PCs) retained was determined based on the scree plot and a threshold of 90% cumulative variance, ensuring the inclusion of the most relevant data while minimising dimensionality. We generated the second set of clustering features comprising the most important PCs.

2.2.3. Clustering

We employed two unsupervised machine learning algorithms—K-means (MacQueen and 1967) and K-medoids (Kaufman and Rousseeuw 2009)—clustering methods on both sets of clustering features: 1) the set of extracted PCs and 2) the set of Euclidean norms of the 360 surface points. The four clustering methods tested in this study include PCA feature-based K-means, PCA feature-based K-medoids, surface mapping-based K-means, and surface mapping-based K-medoids. To identify the optimal number of clusters, the clustering process was repeated multiple times, varying the number of clusters each time. For each additional cluster, the distance between each point and their respective cluster centroid was calculated:

$$D_{i,n} = X_i - \text{ctr}_n \quad (1)$$

In Eq. 1, X_i represents the i th data point, ctr_n is the centroid of the n^{th} cluster, and $D_{i,n}$ is the distance of the i th datapoint to its respective cluster, n . This iterative process ensured that the clustering structure reflected meaningful variations in the dataset. To

validate the selection of the optimal number of clusters, an analysis of variance (ANOVA) test was conducted to assess whether adding an additional cluster resulted in significant differences in distance values compared to the previous cluster configuration (Figure 2). All statistical tests were conducted at a 95% confidence level ($\alpha=0.05$).

The accuracy of each cluster and the clustering methods were evaluated by calculating the sum of squared Euclidean distances between individual surface points and the corresponding centroid of that cluster:

$$D^2(x_i, c_k) = \sum_{k=1}^K \sum_{i=1}^{N_k} (x_i - c_k)^2 \quad (2)$$

In Eq. 2, K is the number of clusters, N_k is the number of points in any given cluster k , x_i is the i th data point, c_k is the cluster centroid, and D is the sum squared Euclidean distance of each cluster and their respective centroid. A lower value of the squared Euclidean distance indicates a better cluster and clustering method.

2.2.4. Modelling and prediction

In order to model the head shapes, we choose NURBS- and Cubic Spline-based methods. In this work, we implemented the interpolation approach to the surface points of each cluster subject, and then the coefficients of the fitted curves were averaged across all subjects within that cluster. The approximation approach was applied to the entire surface point dataset of a cluster without averaging them across subjects. In total, we implemented four modelling

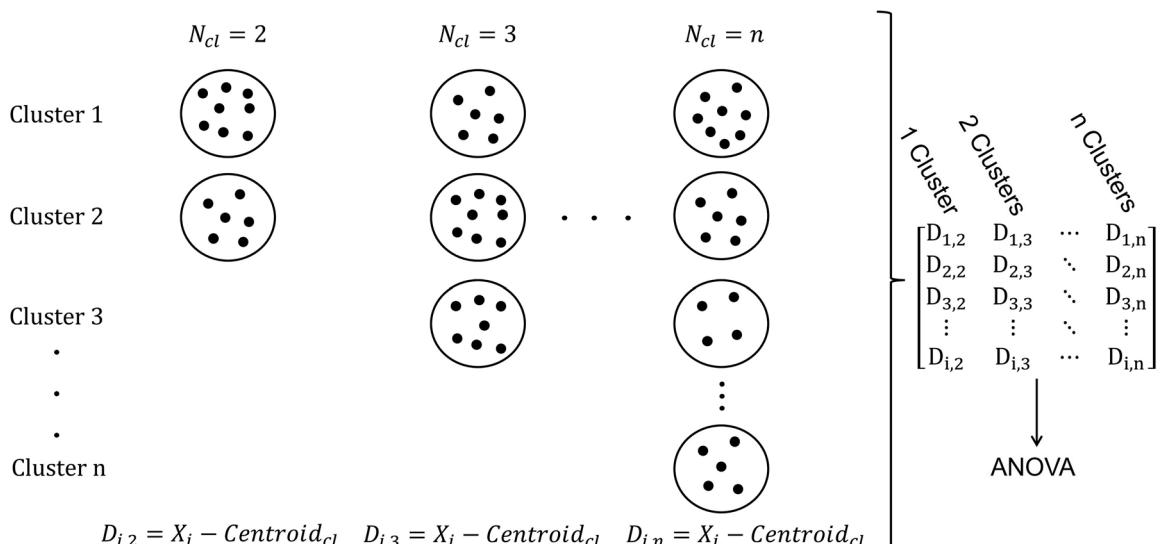


Figure 2. Workflow diagram to calculate the optimal number of clusters using ANOVA. The index “ i ” represents subject number, the index “ n ” represents the total number of clusters and the index “ cl ”, the cluster number.

approaches to derive cluster-specific 18 head curves: 1) NURBS AVG: NURBS with the interpolation function, 2) NURBS LS: NURBS with the LS approximation method, 3) Cubic Spline: the cubic spline method with the interpolation function, and 4) Cubic Spline LS: the cubic spline method with the least square approximation method. The head shape was generated by fitting all 18 predicted head curves of a cluster using all five modelling approaches. The mathematical expression and the details of these approaches are discussed below:

2.2.4.1. NURBS. The NURBS function predicts interpolated points, $C(u)$, which is a weighted sum of control points defined in a parameter space (u) and by a basis function (N) (Piegl and Tiller 1997):

$$C(u) = \sum_{i=1}^n N_{i,p}(u) P_i \quad (3)$$

In Eq. 3, u is a vector that contains the parameterised representation of the points, P_i denotes the i^{th} control point, p is the degree of the spline, and n is the total number of control points. The control points are calculated based on pre-defined points manually selected in the interpolation process. The basis function was computed using the following recursive function (Piegl and Tiller 1997):

$$N_{i,p}(u) = \frac{u - u_i}{u_{i+p} - u_i} N_{i,p-1}(u) + \frac{u_{i+p+1} - u}{u_{i+p+1} - u_{i+1}} N_{i+1,p-1}(u) \quad (4)$$

Note that:

$$N_{i,0}(u) = \begin{cases} 1, & u_i \leq u < u_{i+1} \\ 0, & \text{otherwise} \end{cases} \quad (5)$$

In this approach, we first averaged the 3D surface points of each curve (out of 18 curves) for all subjects within a cluster and then applied the NURBS method to generate a fitted curve.

2.2.4.2. NURBS LS. In the LS approach, the control point was selected by minimising the error—the squared of the difference between the approximated prediction and the 3D data point:

$$\text{minimize } E = \sum_{k=1}^{n-1} \|D_k - C(u)\|^2 \quad (6)$$

where n represents the total number of 3D points, D_k denotes the k^{th} 3D point in the cartesian space and $C(u)$ is an approximated point across all subjects and is

expressed differently than the standard NURBS prediction in Eq. 3:

$$C(u) = N_{1,p}(u) D_1 + \sum_{i=2}^{h-1} N_{i,p}(u) P_i + N_{h,p}(u) D_n \quad (7)$$

In Eq. 7, h , p , P_i , D_1 , and D_n denote the number of control points, the degree of the spline, the i^{th} control point, the first 3D data point, and the last 3D data point, respectively. In this work, we selected six control points as they were reported to show the best performance (i.e., representing the original curvature) in a previous study (Harmening and Neuner 2016) that varied the control points between 1 to 12. Using the concatenated surface points of all subjects within a cluster, we subsequently generated all 18 predicted head curves.

2.2.4.3. Cubic spline. The cubic spline is a representation of continuous segments of cubic polynomials, which are separated by specific points called knots (p). In each of these knots, a new polynomial segment, f , starts with different coefficients (McKinley and Levine 1998):

$$f_{j,k}(p) = a_{j,k} + b_{j,k}(p - P_{j,k}) + c_{j,k}(p - P_{j,k})^2 + d_{j,k}(p - P_{j,k})^3, \quad j=1,\dots,18, k=1,\dots,5 \quad (8)$$

In Eq. 8, $a_{j,k}$, $b_{j,k}$, $c_{j,k}$, and $d_{j,k}$ are the coefficients of k^{th} segment in the j^{th} curve and P_{jk} is the knot coordinate of the k^{th} segment in the j^{th} curve, and $f_{j,k}(p)$ is the k^{th} polynomial segment of j^{th} curve. Before implementing the cubic spline methods, we created an independent parameterised variable (t) to transform all 3D surface points into 1D data points. The transformed 1D data was then normalised across all subjects within a cluster that ranged between 0 and 1:

$$t_{i,s}^c = \begin{cases} 0, & i=1 \\ t_{i-1,s}^c + \frac{\|v_{i,s}^c - v_{i-1,s}^c\|}{\sum_{k=2}^n \|v_{k,s}^c - v_{k-1,s}^c\|}, & 1 < i < n \\ 1, & i=n, \end{cases} \quad (9)$$

In Eq. 9, v_i denotes the i^{th} cartesian 3D data point (x_i, y_i, z_i) of a curve c and subject s . For each curve c , the variable $t_{i,s}^c$ is a transformed 1D vector of size 20×1 . For each cluster and each curve, all $t_{i,s}^c$ vectors were concatenated across subjects to form a unique vector, T . Subsequently, this new parameterised space was used to create new 2D space sets— (\bar{T}, \bar{x}) , (\bar{T}, \bar{y}) , and

(\bar{T}, \bar{z}) —corresponding to each one of the original cartesian 3D data points (x, y, z) .

We selected a total of six-knot points, similar to NURBS' control points, to fit the cubic models (Harmening and Neuner 2016). We first averaged each surface point of a curve across all cluster subjects and then transformed the 3D data points to a 2D parameterised space set c Similar to the NURBS approach, the Cubic Spline function was implemented to the six selected knot points, representing all 20 surface points of a curve, in the new parametrised space in order to generate a fitted cubic spline curve.

2.2.4.4. Cubic spline LS. In the Cubic Spline LS method, instead of averaging the 3D surface points across all subjects, we transformed their 3D surface points to a 2D parameterised space, as expressed in Eq. 9 (the previous section). Then, we implemented the Cubic Spline LS function to fit a curve that minimised the distance between the six approximated knot points and individual parameterised coordinates— (\bar{T}, \bar{x}) , (\bar{T}, \bar{y}) , and (\bar{T}, \bar{z}) , which are the transformed coordinates of the original 3D cartesian data points:

$$\begin{aligned} & \min \|f(T) - X \\ &= \min_{a,b,c,d} \|a + b(T-P) + c(T-P)^2 + d(T-P)^3 - X\| \end{aligned} \quad (10)$$

In Eq. 10, P is the knot point selected in a given segment in the parameterised space, X is the value of the specific coordinate (x, y , or z) in the cartesian space, and a, b, c , and d are the coefficients of the cubic spline to be minimised. We subsequently implemented the Cubic Spline LS approach to generate 18 predicted curves for each cluster. The algorithmic code for this approach is provided in Appendix 1.

2.2.5. Performance measures

Being aware of the dataset's size and gender imbalance, we implemented various performance metrics, such as mean squared error (MSE) and pseudo R-squared (R^2) to ensure the numerical stability, accuracy, and robustness of our methods. The MSE compared model predictions and actual 3D points or head measures:

$$MSE = \frac{1}{n} \sum_{i=1}^n (y_i - \hat{y}_i)^2 \quad (11)$$

where n represents the number of data points, y_i is the subjects' 3D points, and \hat{y}_i is the predicted values from the models. A total mean squared error was also calculated to assess the overall accuracy of the methods across clusters. Additionally, due to the

nonlinearity of the predicted curves, numerical stability and robustness of the shape modelling methods were assessed using pseudo R^2 score to explain the variability of the predicted shape (Eq. 12).

$$R^2 = 1 - \frac{\ln SSR}{\ln SSE} \quad (12)$$

where SSR is the sum of squares of residuals, and SSE is the sum of squared errors. Unlike the traditional R^2 , the pseudo R^2 typically yields lower values, ranging from 0.2 to 0.4, for a good fit (McFadden 1973). In addition, as the methods may achieve similar MSE and R^2 scores, the run time to perform each method was also considered to determine the most effective method.

The most effective curve fitting and clustering techniques were selected to generate the representative head shapes and the descriptive statistics, such as mean, standard deviation, minimum and maximum values, and the 5th and 95th percentiles of their primary head anthropometric features—bzygomatic breadth (BB), head circumference (HC), and head length (HL) in accordance with the definitions specified in the ANSUR II database (Paquette 2009)—were calculated and compared with those from four widely-used anthropometric databases: ANSUR II (Paquette 2009), CAESAR (Zhuang, Landsittel, et al. 2010), NIOSH (Zhuang and Bradtmiller 2005), and US Army (Gordon 1988; Zhuang and Bradtmiller 2005). Additionally, we performed a point-to-point similarity analysis between these four predicted head shapes and five NIOSH digital head forms—small, short-wide, medium, long narrow, and large head shapes (Zhuang, Benson, et al. 2010)—using the 3D deviation analysis tool in the Geomagic Essentials platform and then categorising them as corresponding standard head form sizes. These NIOSH digital head forms were generated from the Zhuang and Bradtmiller (2005) study of head and facial dimensions from 3,997 US respirator users (2543 males and 1454 females).

3. Results

3.1. Dimensionality reduction and clustering

The scree plot of the PCA analysis revealed that seven PCs collectively contributed over 90% of the total data variation (Figure 3). Thus, the PCA feature-based K-means and K-medoids clustering processes were performed using these seven PCA-reduced dimensions, as well as our proposed surface mapping-based representation of the complex 3D head shape. The surface

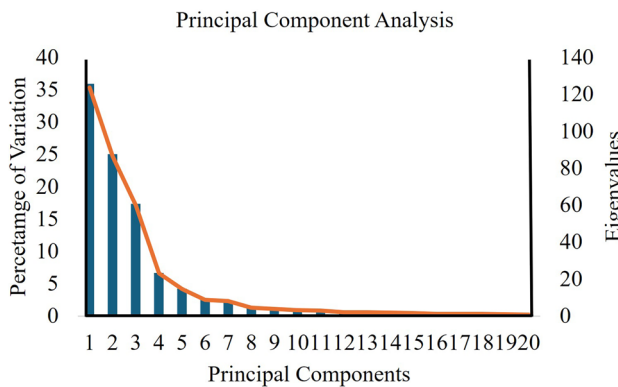


Figure 3. Scree plot of principal component analysis process. The X-axis represents the total number of principal components (PCs), and the Y-axis indicates the percentage of total variance explained by each PC.

Table 1. ANOVA results (F - and p -values) for determining the optimal number of clusters.

	F -Value	F Critical	p -Value
Number of clusters	2	1.74	3.95
	3	2.82	3.07
	4	3.93	2.6
			0.1919
			0.0641
			0.0099

mapping-based K-means method showed the lowest squared Euclidean distance (34.39 ± 15.41), about 17.65, 24.48, and 53.86% lower than that of surface mapping-based K-medoids (41.76 ± 15.23), PCA feature-based K-means (45.54 ± 11.37), and PCA feature-based K-medoids (74.54 ± 13.09), respectively (Figure 4). Furthermore, both surface mapping and the PCA-based K-means clustering method performed better than surface mapping and PCA-based K-medoids, showing about 17.65 and 38.91% smaller squared Euclidean distances, respectively. Overall, data clustering based on the 360 surface points yielded lower squared Euclidean distances than the PCA-based data clustering method, suggesting that the PCA-based reduced dimensions may not accurately represent a complex, uneven head shape.

Therefore, we selected the surface mapping-based K-means clustering results to proceed with further analyses: cluster selection, shape modelling, and shape prediction. The ANOVA results (Table 1) for the surface mapping-based K-means clustering yielded a total of four optimal clusters (F -value = 3.93, p -value = 0.009): Cluster 1 with one male and six females ($n=7$), Cluster 2 with only three males ($n=3$), Cluster 3 with 13 males and three females ($n=16$), and Cluster 4 with seven males and three females ($n=10$). A schematic presentation of four predicted head shapes is provided in Figure 5. Shape 1 had the smallest head circumference and followed by Clusters 3 and 4. On the other

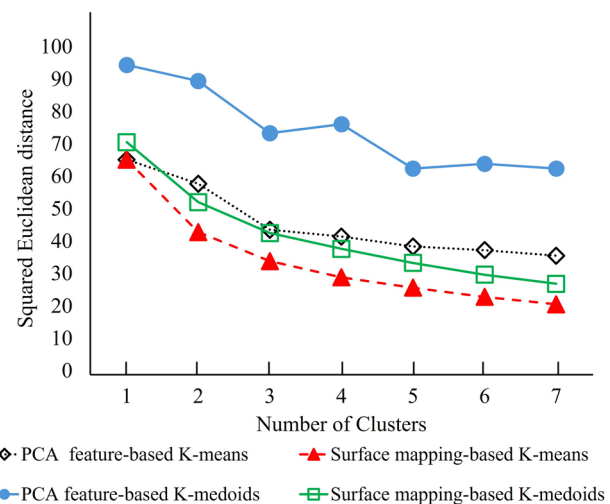


Figure 4. Performance measures of clustering methods. The clustering method was performed using K-means and K-medoids unsupervised machine learning algorithms on the reduced dimensions of the 3D complex, uneven head shape. The dimensionality reduction was performed using principal component analysis (PCA) and our proposed method on a selection of 360 surface points (surface mapping).

hand, Cluster 2 had the largest head circumference measures, with a clearly larger occipital region compared to other clusters.

3.2. Shape modeling methods

Among four shape modelling techniques, the lowest MSE values were observed for the Cubic Spline LS ($MSE = 0.70$) (Table 2), with an average reduction of 6.67, 90.26, and 33.82% compared to NURBS ($MSE = 0.75$), NURBS LS ($MSE = 7.19$), and Cubic Spline ($MSE = 2.07$) methods, respectively. Likewise, the pseudo-r-squared values (R^2) of the Cubic Spline LS method showed the highest R^2 value (Table 3), with an R^2 of about 1.13, 67.08, and 22.83% higher than those of the NURBS, NURBS LS, and Cubic Spline methods, respectively (Table 2). The average computational time for the Cubic Spline LS method (0.14 seconds) was also the lowest among all methods (Table 3).

3.3. Head shape prediction and size identification

As aforementioned, the surface mapping-based K-means clustering and the Cubic Spline LS method were found to be the most efficient and accurate methods for shape clustering and modelling, we utilised them to generate four cluster-specific head shapes: Shape 1, Shape 2, Shape 3, and Shape 4 from Cluster 1, Cluster 2, Cluster 3, and Cluster 4 datasets, respectively. The anthropometric measures of these

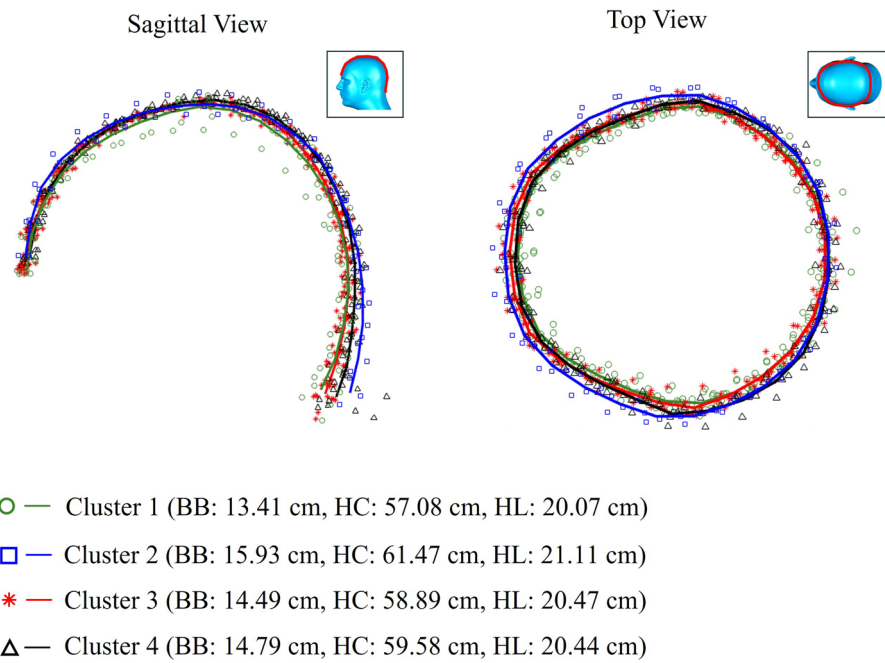


Figure 5. Sagittal and top views of Clusters 1-4 as determined using surface mappings-based K-means clustering algorithm. Dots indicate subjects' 2D head points, while solid lines indicate the cluster average. The dimensions of head anthropometric features—bzygomatic breadth (BB), head circumference (HC), and head length (HL) estimated in accordance with the definitions specified in the ANSUR II database (Paquette 2009)—are in centimetres.

Table 2. Mean squared error values (cm^2) of four shape modelling methods used in this study.

	Cluster 1 (n=7)	Cluster 2 (n=3)	Cluster 3 (n=16)	Cluster 4 (n=10)	Average MSE
NURBS	0.54 ± 0.46	1.34 ± 1.12	0.62 ± 0.66	0.51 ± 0.35	0.75
NURBS LS	7.18 ± 2.27	5.28 ± 2.28	8.60 ± 2.25	7.69 ± 2.38	7.19
Cubic spline	1.91 ± 1.05	2.67 ± 1.99	1.92 ± 1.30	1.80 ± 0.59	2.07
Cubic spline LS	0.51 ± 0.40	1.19 ± 0.68	0.60 ± 0.59	0.50 ± 0.39	0.70

Table 3. Pseudo R^2 and computational time (in seconds) results of four shape modelling methods used in this study

	Cluster 1 (n=7)	Cluster 2 (n=3)	Cluster 3 (n=16)	Cluster 4 (n=10)	Average	Computational time (s)
NURBS	0.316	0.240	0.256	0.253	0.266 ± 0.034	1.54
NURBS LS	0.172	0.179	0.173	0.119	0.161 ± 0.028	1.87
Cubic spline	0.233	0.191	0.203	0.248	0.219 ± 0.026	0.26
Cubic spline LS	0.320	0.244	0.265	0.246	0.269 ± 0.035	0.14

predicted shapes were compared with their corresponding 5th, 50th, and 95th percentile measurements from four prominent anthropometric databases (Table 4). Additionally, a point-to-point deviation analysis was conducted using NIOSH head forms to compare them with the representative head forms of the 3D shape-based clusters generated using the Cubic Spline LS method (Figure 6). Shape 1 presented anthropometric measures that were closely aligned with the average (50th percentile) population measures across all databases, particularly for HC and HL (Table 4). BB ranged from the 18th to 37th percentile, suggesting a slightly narrower head width, but overall, Shape 1 was

shown to represent the average population (50th percentile or medium) head shape. The minimal average point-to-point deviation ($-0.07 \text{ cm} \approx 0$) from the NIOSH Medium head form ensured Shape 1's representation with a medium-sized, average population dataset (Figure 6). Shape 2 was consistently aligned with the 99th percentile across all databases and all measures, indicating it represents an extremely large-size individual. This interpretation was reinforced by the substantial negative deviation (-0.41 cm), even from the NIOSH Large head form, suggesting that Shape 2 exceeds standard large references and may require a double extra-large classification. Shape 3 demonstrated

Table 4. Comparison of head measurements for each cluster across four databases (ANSUR II, CAESAR, NIOSH, and US Army).

BB (cm)	ANSUR II (Paquette 2009)			CAESAR (Zhuang, Landsittel, et al. 2010)			NIOSH (Zhuang and Bradtmiller 2005)			US Army (Gordon 1988; Zhuang and Bradtmiller 2005)		
	5th	50th	95th	5th	50th	95th	5th	50th	95th	5th	50th	95th
	12.80	13.97	15.20	12.97	14.42	15.87	12.93	14.04	15.16	12.78	13.66	14.54
Shape 1	13.41 (28th)			13.41 (18th)			13.41 (24th)			13.41 (37th)		
Shape 2	15.93 (99th)			15.93 (99th)			15.93 (99th)			15.93 (99th)		
Shape 3	14.49 (69th)			14.49 (52nd)			14.49 (68th)			14.49 (92nd)		
Shape 4	14.79 (80th)			14.79 (61st)			14.79 (80th)			14.79 (99th)		
HC (cm)	ANSUR II (Paquette 2009)			CAESAR (Zhuang, Landsittel, et al. 2010)			NIOSH (Zhuang and Bradtmiller 2005)			US Army (Gordon 1988; Zhuang and Bradtmiller 2005)		
	5th	50th	95th	5th	50th	95th	5th	50th	95th	5th	50th	95th
	54.00	57.00	60.00	53.36	56.78	60.19	53.96	56.81	59.67	53.29	55.74	58.18
Shape 1	57.08 (51st)			57.08 (54th)			57.08 (54th)			57.08 (74th)		
Shape 2	61.47 (99th)			61.47 (99th)			61.47 (99th)			61.47 (99th)		
Shape 3	58.89 (78th)			58.89 (77th)			58.89 (83rd)			58.89 (99th)		
Shape 4	59.58 (89th)			59.58 (87th)			59.58 (94th)			59.58 (99th)		
HL (cm)	ANSUR II (Paquette 2009)			CAESAR (Zhuang, Landsittel, et al. 2010)			NIOSH (Zhuang and Bradtmiller 2005)			US Army (Gordon 1988; Zhuang and Bradtmiller 2005)		
	5th	50th	95th	5th	50th	95th	5th	50th	95th	5th	50th	95th
	18.20	19.63	21.00	20.83	22.94	25.05	18.17	19.37	20.58	18.08	19.12	20.16
Shape 1	20.07 (64th)			20.07 (1st)			20.07 (76th)			20.07 (91st)		
Shape 2	21.11 (99th)			21.11 (99th)			21.11 (99th)			21.11 (99th)		
Shape 3	20.47 (78th)			20.47 (1st)			20.47 (91st)			20.47 (99th)		
Shape 4	20.44 (77th)			20.44 (1st)			20.44 (89th)			20.44 (99th)		

The values in parentheses indicate the percentile ranking of each cluster's measurement within each respective database.

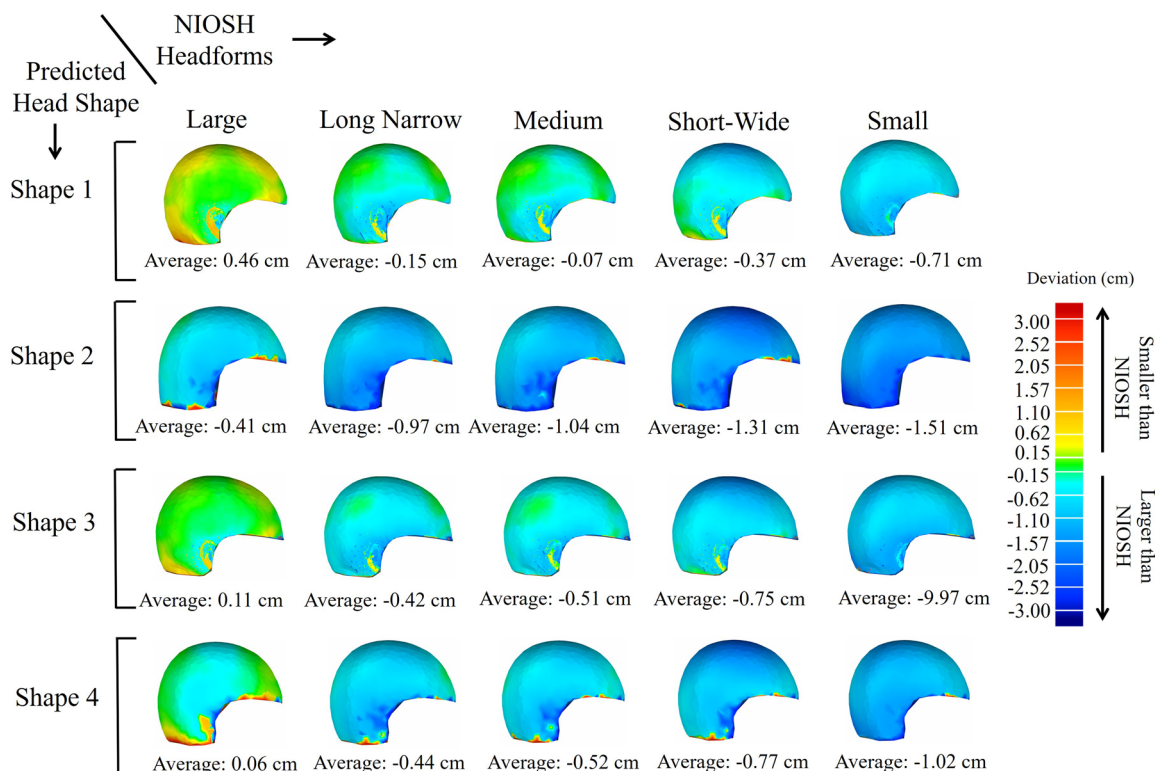


Figure 6. Similarity analyses (point-to-point distance and standard deviation) in Geomagic Essentials platform between predicted head shapes and five NIOSH 3D head forms: small, short-wide, medium, long-narrow, and large sizes. Warmer colours, i.e., more to the red (>0 ; positive deviation), indicated regions in our head shapes that were smaller than the corresponding regions of the NIOSH head forms, while colder colours, more to the blue (<0 ; negative deviation), highlighted regions that were larger. A greener colour, i.e., more to the centre, referred to regions with perfect matching between the predicted head shapes and the NIOSH head form.

moderate anthropometric dimensions. Its value fell between the 52 and 92nd percentiles, depending on the measure and database, indicating a larger-than-average but not extreme (i.e., more than the 92nd percentile) head shape. The average point-to-point deviation (0.11 cm) from the NIOSH Large form suggests it was generally consistent with a large head form. Shape 4 also fell in the upper percentile ranges (61st to 99th), particularly for BB and HC, and closely matched the 99th percentile in the US Army dataset for all dimensions. The overall point-to-point deviation (0.06 cm) from the NIOSH Large form was modest, with good regional conformity in the occipital and frontal zones. However, bluer colour marks in occipital and temporal regions suggest that the shape was broader in those areas. Consequently, we can classify Shape 4 as an extra-large head shape. Overall, all four predicted head shapes based on our acquired firefighter data exhibit distinct anthropometric profiles, with Shape 1 representing individuals of medium size, Shape 3 representing those of large size, Shape 4 representing those of extra-large size, and Shape 2 representing those of double extra-large size heads.

4. Discussion

This study aimed to develop representative head shapes for firefighters by employing advanced clustering techniques and shape modelling methods. Results showed that our proposed surface mapping (can be called a data and dimensionality reduction technique too), K-means clustering, and Cubic Spline LS methods provided an efficient and accurate methodological framework for predicting head shapes based on 3D scan data from small populations or specialised occupational groups (Figures 3, 4, Tables 1, 2, 3).

In general, PCA reduces dimensionality by capturing linear patterns of data variation (via eigenvectors) and may consequently fail to capture the inherent nonlinearities and local geometric intricacies of complex 3D head shapes (Jolliffe 2002). On the contrary, the explicit modelling of 360 spatial coordinates across the entire head surface may have preserved the detailed geometric features and local curvatures of the head while also capturing subtle subject-specific morphological variations in head geometry. Thus, our proposed clustering algorithm on the mapped surface, i.e., 360 surface points, outperformed the PCA method in characterising the complex 3D head scan data. Among clustering techniques, K-means outperformed K-medoids, as indicated by its lower squared Euclidean distance compared to K-medoids clustering. The K-means approach calculates cluster centroids by averaging all data points

within each cluster, thereby making it sensitive to outliers in small datasets. On the other hand, the K-medoids approach selects actual data points as cluster centroids, making it less effective in capturing data variance in small datasets. However, with an increase in the sample size, the distribution of the sample mean approaches normality, and the centroid aligns more closely with the true mean. This characteristic may make K-medoids advantageous for large datasets, as it avoids computationally intensive averaging processes at each iteration and reduces processing time (Madhulatha 2011). Conversely, for small datasets, K-means can outperform K-medoids due to its ability to better capture variations, which was evident in this study.

Among shape modelling techniques, the Cubic Spline LS method demonstrated superior accuracy (the lowest MSE and highest R^2 values) and computational efficiency (the least processing time) compared to the NURBS, NURBS LS, and standard Cubic Spline methods. On the contrary, we observed higher MSE and lower R^2 values for both NURBS methods, which can be attributed to the second-order continuity of NURBS curves. While this continuity ensures smoother transitions and higher curvature gradients, it introduces increased oscillations (Kuželka and Marušák 2014), which, in turn, elevates the error during curve fitting. Among both NURBS methods, the standard NURBS exhibited relatively better MSE and R^2 values than the NURBS LS method, as averaging the data points in standard NURBS reduces variability and mitigates oscillations that typically contribute to higher error values in small datasets. Additionally, the flexibility of the NURBS methods in customising shape designs comes with an increased computational load due to the necessity of handling more parameters, such as knots and control points (Piegl 1991; Dimas and Briassoulis 1999). In contrast, Cubic Splines provide a simpler and more efficient solution for applications where computational resources are limited and the need for detailed design modification is less critical. They are faster to implement and provide satisfactory accuracy, making them well-suited for scenarios where speed and computational efficiency are prioritised. Interestingly, the standard Cubic Spline applied to the average surface points did not perform better than the NURBS method. This discrepancy in their performances is likely due to the inherently minimal curvature of cubic splines when interpolating data points, which leads to less flexibility in fitting the data and ultimately results in lower accuracy compared to the NURBS approach (Lahtinen 1988; Ma and Kruth 1998; mCarlson 2009). Despite the limitations associated with standard Cubic Splines, the Cubic Spline LS method outperformed both NURBS

methods. This suggests that the Cubic Spline LS uses cubic polynomial segments combined with least squares optimisation, offering sufficient curve flexibility without excessive curvature fluctuations. By incorporating all data points in the fitting process rather than a reduced or average dataset, Cubic Spline LS maintains accuracy while effectively mitigating data variability that originated from various sources, such as subject-specific variations in head anthropometry, gender imbalance, etc (Lahtinen 1988).

Comparative analysis of the predicted head shapes against established anthropometric databases revealed distinctive characteristics among the clusters. In this study, the average bizygomatic breadth, head circumference, and head length of firefighters were found to be larger than those reported in other studies that collected general population data (Zhuang, Benson, et al. 2010; Zhuang, Landsittel, et al. 2010; Perret-Ellena et al. 2015; Kuo, Wang, and Lu 2020). Notably, our data closely aligned with the most recent military personnel dataset (ANSUR II (Paquette 2009)), while significant deviations were observed when compared to the older U.S. military dataset (Gordon 1988) collected three decades ago. This discrepancy may reflect generational anthropometric changes driven by improved nutrition and lifestyle (Goleij, Hafezi, and Ahmadi 2024), underscoring the importance of updating anthropometric datasets, especially for designing helmets and occupational gears for physically demanding occupations like firefighting, police officers, and military personnels (Henderson 2010; Taylor et al. 2015). Additionally, our dataset showed overall larger measurements compared to the CAESAR dataset, which comprises American and European civilian populations. This finding aligns with previous research (Hsiao, Long, and Snyder 2002; Hsiao, Weaver, et al. 2014; Hsiao, Whitestone, et al. 2014) indicating that the anthropometric characteristics of physically demanding occupations, such as those of firefighters and law enforcement officers, differ from those of the general population. For example, firefighters are generally heavier than the average U.S. civilian, with an 8–10 kg higher weight on average. Although our study did not study the correlation between BMI and head anthropometric measures, prior research (Henneberg and Ulijaszek 2010) has indicated that a higher weight and BMI are directly associated with larger head dimensions, such as head circumference. These observations highlight the necessity of collecting occupation-specific anthropometric data to design head-mounted devices that better fit the unique needs of these specialised populations.

Several limitations must be acknowledged in this study. First, the anthropometric measures of the

predicted shapes were manually extracted in the Geomagic software, introducing potential measurement errors that could impact shape/cluster classification. Second, the ear was used as the reference point for trimming the head scans. This approach resulted in some variability, as certain head scans displayed longer occipital regions than others. Such discrepancies could affect the accuracy of the 3D shape-based clustering method, as they may cause heads to be assigned to larger or smaller clusters depending on the size of the ears. Fourth, our final participant cohort consisted of 25 males and 11 females. It is important to highlight that, though the firefighter population is predominantly comprised of males, a gender-balanced cohort could have provided a different cluster or shape distribution. Given that the dataset's small size and gender imbalance could contribute to total data variation, we implemented optimisation-based LS approximation techniques into the Cubic Spline and B-spline methods to find the best-fit curves/shapes. Additionally, we evaluated the performance of our methods using metrics like MSE and pseudo-R² measures in order to ensure their accuracy and robustness. Fifth, our primary goal was to propose a methodological framework and clustering and shape modelling methods that can be readily implemented on small datasets and in resource-limited settings, not to construct a comprehensive database. Therefore, future works can focus on implementing our proposed framework and methodologies on larger datasets with a more balanced representation of male and female participants. Sixth, the trimming process focused specifically on the region covered by the helmet, which included the ear and occipital areas. As a result, certain details of the frontal region, such as the nose and eyes, were excluded, which may have affected the clustering process and the overall representation of the head shape. Seventh, although most anthropometric databases demonstrate head anthropometry and 3D head form representation, such as the NIOSH head forms, by using 1-D head measures (e.g., bizygomatic breadth, head breadth, head circumference, head length, tragion-to-top-of-the-head distance, and sagittal arc), some previous studies attempted to include additional facial features in their head anthropometry study. Given that this research is part of a broader project focused on developing head-mounted helmets, we maintained our focus on 3D head modelling using features that are primarily relevant to the head scalp and skull regions. Finally, this study did not aim primarily to replace existing methodologies well-established for large civilian databases; rather, its primary objective was to determine clustering and shape modelling methods, as well as a computational modelling framework,

suitable for small datasets, such as those from firefighters, law enforcement officers, and fighter pilots, acquired in resource-limited settings. However, it is noteworthy to mention that the appropriateness of these methods should be studied for large civilian datasets in the future.

In summary, predicting head shapes using a small dataset is challenging, as the existence of data outliers may adversely impact modelling accuracy. To the best of our knowledge, no previous work has focused on small datasets. Our results demonstrated that the combination of K-means clustering alongside the Cubic Spline LS shape modelling method is effective for handling small sample sizes and provides an accurate solution for population-specific anthropometric analysis. The proposed methodological framework offers a promising approach to enhance clustering and shape modelling accuracy, particularly in cases where large datasets are impractical to collect, making it especially beneficial for population-specific anthropometric applications.

Acknowledgments

We acknowledge the U.S. Department of Homeland Security (Award # 70RSAT21CB0000023) for supporting this study. Additionally, we would like to thank the local firefighters for participating in this study.

Authors' contribution

Leonardo H. Wei, B.S.: Conceptualisation, Methodology, Data Collection and Preparation, Writing. S. Sudeesh, Ph.D.: Writing, Editing, Data Analysis. Sajal Chakroborty, Ph.D.: Conceptualisation, Writing, and Reviewing. Suman K. Chowdhury, Ph.D.: Supervision, Funding Acquisition, Investigation, Reviewing, and Editing.

Disclosure statement

The authors declare no competing interests.

Funding

The work was supported by the U.S. Department of Homeland Security's Science & Technology Directorate under the award # 70RSAT21CB0000023.

ORCID

S. Sudeesh  <http://orcid.org/0000-0003-2644-8113>

Suman K. Chowdhury  <http://orcid.org/0000-0003-4067-3472>

References

- Amor, BB., M. Ardabilian, and L. Chen **2006**. An improved 3D human face reconstruction approach based on cubic splines models. Third International Symposium on 3D Data Processing, Visualization, and Transmission (3DPVT'06), IEEE.
- Ball, RM. **2011**. SizeChina: A 3D anthropometric survey of the Chinese head.
- Boehnen, C., and P. Flynn. **2005**. Accuracy of 3D scanning technologies in a face scanning scenario. Fifth International Conference on 3-D Digital Imaging and Modeling (3DIM'05), IEEE.
- Bougourd, J., P. Treleaven, and RM. Allen. **2004**. The UK national sizing survey using 3d body scanning. Eurasia-Tex Conference, Donghua University, Shanghai, China.
- Bruneau, DA., and DS. Cronin. **2020**. "Head and Neck Response of an Active Human Body Model and Finite Element Anthropometric Test Device during a Linear Impactor Helmet Test." *Journal of Biomechanical Engineering* 142 (2): 021004. doi:[10.1115/1.4043667](https://doi.org/10.1115/1.4043667).
- Dimas, E., and D. Briassoulis. **1999**. "3D Geometric Modelling Based on NURBS: A Review." *Advances in Engineering Software* 30 (9-11): 741–751. doi:[10.1016/S0965-9978\(98\)00110-0](https://doi.org/10.1016/S0965-9978(98)00110-0).
- Dong, Y., Y. Zhao, S. Bai, G. Wu, and B. Wang. **2010**. "Three-Dimensional Anthropometric Analysis of the Chinese Nose." *Journal of Plastic, Reconstructive & Aesthetic Surgery: JPRAS* 63 (11): 1832–1839. doi:[10.1016/j.bjps.2009.11.035](https://doi.org/10.1016/j.bjps.2009.11.035).
- Ellena, T., A. Subic, H. Mustafa, and T. Yen Pang. **2018**. "A Novel Hierarchical Clustering Algorithm for the Analysis of 3D Anthropometric Data of the Human Head." *Computer-Aided Design and Applications* 15 (1): 25–33. doi:[10.1080/16864360.2017.1353727](https://doi.org/10.1080/16864360.2017.1353727).
- Ellena, T., S. Skals, A. Subic, H. Mustafa, and TY. Pang. **2017**. "3D Digital Headform Models of Australian Cyclists." *Applied Ergonomics* 59 (Pt A): 11–18. doi:[10.1016/j.apergo.2016.08.031](https://doi.org/10.1016/j.apergo.2016.08.031).
- Fu, F., A. Luximon, and Y. Luximon. **2024**. "3D Human Ear Modelling with Parameterization Technique and Variation Analysis." *Ergonomics* 67 (5): 638–649. doi:[10.1080/00140139.2023.2236820](https://doi.org/10.1080/00140139.2023.2236820).
- Goleij, N., P. Hafezi, and O. Ahmadi. **2024**. Investigating the trends and causes of changes in human anthropometric dimensions over the past three decades: a challenge for ergonomic design. *International Journal of Occupational Safety and Ergonomics* 30 (2): 480–485. doi:[10.1080/1080548.2024.2318945](https://doi.org/10.1080/1080548.2024.2318945).
- Gordon, CC. **1988**. Anthropometric survey of US army personnel: methods and summary statistics. Technical Report Natick/TR-89/044.1989.
- Hadi, NA., and N. Alias. **2019**. 3-dimensional human head reconstruction using cubic spline surface on CPU-GPU platform. Proceedings of the 2019 4th International Conference on Intelligent Information Technology.
- Harmening, C., and H. Neuner. **2016**. Using model selection criteria to determine the optimal number of B-spline control points for areal deformation modelling. Proceedings of the 3rd Joint International Symposium on Deformation Monitoring (JISDM), Vienna, Austria.
- Henderson, ND. **2010**. "Predicting Long-Term Firefighter Performance from Cognitive and Physical Ability Measures." *Personnel Psychology* 63 (4): 999–1039. doi:[10.1111/j.1744-6570.2010.01196.x](https://doi.org/10.1111/j.1744-6570.2010.01196.x).
- Henneberg, M., and SJ. Ulijaszek. **2010**. "Body Frame Dimensions Are Related to Obesity and Fatness: lean Trunk Size, Skinfolds, and Body Mass Index." *American Journal of*

- Human Biology: The Official Journal of the Human Biology Council* 22 (1): 83–91. doi:10.1002/ajhb.20957.
- Heutinck, Pam, Paul Knoops, Naiara Rodriguez Florez, Benedetta Biffi, William Breakey, Greg James, Maarten Koudstaal, Silvia Schievano, David Dunaway, Owase Jeelani, and Alessandro Borghi. 2021. "Statistical Shape Modelling for the Analysis of Head Shape Variations." *Journal of Cranio-Maxillo-Facial Surgery: official Publication of the European Association for Cranio-Maxillo-Facial Surgery* 49 (6): 449–455. doi:10.1016/j.jcms.2021.02.020.
- Hsiao, H., D. Long, and K. Snyder. 2002. "Anthropometric Differences among Occupational Groups." *Ergonomics* 45 (2): 136–152. doi:10.1080/00140130110115372.
- Hsiao, H., D. Weaver, J. Hsiao, J. Whitestone, T-Y. Kau, R. Whisler, and R. Ferri. 2014. "Comparison of Measured and Self-Reported Anthropometric Information among Firefighters: implications and Applications." *Ergonomics* 57 (12): 1886–1897. doi:10.1080/00140139.2014.952351.
- Hsiao, H., J. Whitestone, T-Y. Kau, R. Whisler, JG. Routley, and M. Wilbur. 2014. "Sizing Firefighters: method and Implications." *Human Factors* 56 (5): 873–910. doi:10.1177/0018720813516359.
- Hsiao, H., R. Whisler, and B. Bradtmiller. 2023. "Needs and Procedures for a National Anthropometry Study of Law Enforcement Officers." *Human Factors* 65 (3): 403–418. doi:10.1177/00187208211019157.
- Huang, Y., Zhu, Z. Zhu, J. Ye, M. Zhang, K. Huang, Y. ZHU Z. ZHU J. YE M, and Zhang, K. 2023. "A Morphometric Study of Head in the Population of Young Chinese Adults." *International Journal of Morphology* 41 (3): 873–880. doi:10.4067/S0717-95022023000300873.
- Isaacs, M. 2005. "3D Fit for the Future-3D Fit and Design Can be the Solution to Several Industry Problems." *AATCC Review-American Association of Textile Chemists and Colorists* 5 (12): 21–24.
- Jasper, HH. 1958. "Ten-Twenty Electrode System of the International Federation." *Electroencephalography and Clinical Neurophysiology*. 10: 371–375.
- Jolliffe, IT. 2002. *Principal Component Analysis for Special Types of Data*. New York, USA: Springer.
- Kaufman, L., and PJ. Rousseeuw. 2009. *Finding Groups in Data: An Introduction to Cluster Analysis*. New Jersey, USA: John Wiley & Sons.
- Kuo, C-C., M-J. Wang, and J-M. Lu. 2020. "Developing Sizing Systems Using 3D Scanning Head Anthropometric Data." *Measurement* 152: 107264. doi:10.1016/j.measurement.2019.107264.
- Kuželka, K., and R. Marušák. 2014. "Comparison of Selected Splines for Stem Form Modeling: A Case Study in Norway Spruce." *Annals of Forest Research* 0 (0): 1. doi:10.15287/afr.2014.177.
- Lacko, D., T. Huysmans, J. Vleugels, G. De Bruyne, MM. Van Hulle, J. Sijbers, and S. Verwulgen. 2017. "Product Sizing with 3D Anthropometry and k-Medoids Clustering." *Computer-Aided Design* 91: 60–74. doi:10.1016/j.cad.2017.06.004.
- Lacko, D., T. Huysmans, PM. Parizel, G. De Bruyne, S. Verwulgen, MM. Van Hulle, and J. Sijbers. 2015. "Evaluation of an Anthropometric Shape Model of the Human Scalp." *Applied Ergonomics* 48: 70–85. doi:10.1016/j.apergo.2014.11.008.
- Lahtinen, A. 1988. On the construction of monotony preserving taper curves.
- Liu, K., Y. Yan, K. Zeng, and H. Wang. 2025. "Statistical Shape Analysis of the Chinese External Ear for Ergonomic Design of in-Ear Products." *Ergonomics*: 1–20. doi:10.1080/00140139.2025.2458631.
- Luximon, A., Y. Zhang, Y. Luximon, and M. Xiao. 2012. "Sizing and Grading for Wearable Products." *Computer-Aided Design* 44 (1): 77–84. doi:10.1016/j.cad.2011.07.004.
- Luximon, Y., NJ. Martin, R. Ball, and M. Zhang. 2016. "Merging the Point Clouds of the Head and Ear by Using the Iterative Closest Point Method." *International Journal of the Digital Human* 1 (3): 305–317. doi:10.1504/IJDH.2016.079888.
- Luximon, Y., R. Ball, and L. Justice. 2012. "The 3D Chinese Head and Face Modeling." *Computer-Aided Design* 44 (1): 40–47. doi:10.1016/j.cad.2011.01.011.
- Ma, L., and J. Niu. 2021. "Three-Dimensional (3D) Anthropometry and Its Applications in Product Design." In *Handbook of Human Factors and Ergonomics*. 281–302. New Jersey, USA: John Wiley & Sons.
- Ma, W., and J-P. Kruth. 1998. "NURBS Curve and Surface Fitting for Reverse Engineering." *The International Journal of Advanced Manufacturing Technology* 14 (12): 918–927. doi:10.1007/BF01179082.
- MacQueen, J. 1967. Some methods for classification and analysis of multivariate observations. Proceedings of the Fifth Berkeley Symposium on Mathematical Statistics and Probability, Oakland, CA, USA.
- Madhulatha, TS. 2011. Comparison between k-means and k-medoids clustering algorithms. International Conference on Advances in Computing and Information Technology; Springer.
- Malkoc, İ., MD. Kaya, O. Erdogan, A. Kara, H. Yesilyurt, and B. Ozkan. 2014. "Are New Generations Getting Bigger in Size? Anthropometric Measurements in Erzurum." *The Eurasian Journal of Medicine* 46 (3): 192–197. doi:10.5152/eajm.2014.54.
- Mandolini, M., M. Caragiuli, A. Brunzini, A. Mazzoli, and M. Pagnoni. 2020. A procedure for designing custom-made implants for forehead augmentation in people suffering from Apert syndrome. *Journal of Medical Systems* 44: 1–10. doi:10.1007/s10916-020-01611-9.
- mCarlson, N. 2009. NURBS surface fitting with Gauss-Newton.
- McFadden, D. 1973. Conditional logit analysis of qualitative choice behavior.
- McKinley, S., and M. Levine. 1998. "Cubic Spline Interpolation." *College of the Redwoods* 45 (1): 1049–1060.
- Molenbroek, J., TJ. Albin, and P. Vink. 2017. "Thirty Years of Anthropometric Changes Relevant to the Width and Depth of Transportation Seating Spaces, Present and Future." *Applied Ergonomics* 65: 130–138. doi:10.1016/j.apergo.2017.06.003.
- Nainggolan, R., R. Perangin-angin, E. Simarmata, and AF. Tarigan 2019. Improved the performance of the K-means cluster using the sum of squared error (SSE) optimized by using the Elbow method. *Journal of Physics: Conference Series*, 1361(1): 012015. IOP Publishing.
- NIOSH 2020. NIOSH Anthropometric Data and ISO Digital Headforms. [accessed]. <https://www.cdc.gov/niosh/data/datasets/rd-10130-2020-0/default.html>.
- Niu, J., and Z. Li. 2012. "Using Three-Dimensional (3d) Anthropometric Data in Design." In *Handbook of Anthropometry: Physical Measures of Human Form in Health and Disease*. 3001–3013. New York, USA: Springer.
- Niu, J., Z. Li, and G. Salvendy. 2009. "Multi-Resolution Shape Description and Clustering of Three-Dimensional Head Data." *Ergonomics* 52 (2): 251–269. doi:10.1080/00140139.200802334561.

- Osborne, JW., and A. Overbay. 2004. "The Power of Outliers (and Why Researchers Should Always Check for Them)." *Practical Assessment, Research, and Evaluation* 9 (1): 6.
- Ostertagová, E. 2012. "Modelling Using Polynomial Regression." *Procedia Engineering* 48: 500–506. doi:[10.1016/j.proeng.2012.09.545](https://doi.org/10.1016/j.proeng.2012.09.545).
- Pal, P., and R. Ballav. 2007. "Object Shape Reconstruction through NURBS Surface Interpolation." *International Journal of Production Research* 45 (2): 287–307. doi:[10.1080/00207540600688481](https://doi.org/10.1080/00207540600688481).
- Paquette, S. 2009. "Anthropometric Survey (ANSUR) II Pilot Study: methods and Summary Statistics." Anthrotch, US Army Natick Soldier Research, Development and Engineering Center.
- Perret-Ellena, T., SL. Skals, A. Subic, H. Mustafa, and TY. Pang. 2015. "3D Anthropometric Investigation of Head and Face Characteristics of Australian Cyclists." *Procedia Engineering* 112: 98–103. doi:[10.1016/j.proeng.2015.07.182](https://doi.org/10.1016/j.proeng.2015.07.182).
- Piegls, L. 1991. "On NURBS: A Survey." *IEEE Computer Graphics and Applications* 11 (1): 55–71. doi:[10.1109/38.67702](https://doi.org/10.1109/38.67702).
- Piegls, L., and W. Tiller. 1997. *The NURBS Book*. Berlin, Heidelberg, Germany: Springer Science & Business Media.
- Ray, S., and RH. Turi. 1999. Determination of number of clusters in k-means clustering and application in colour image segmentation. Proceedings of the 4th International Conference on Advances in Pattern Recognition and Digital Techniques, Calcutta, India.
- Robinette, KM., S. Blackwell, H. Daanen, M. Boehmer, S. Fleming, T. Brill, D. Hoeferlin, and D. Burnsides. 2002. *Civilian American and European Surface Anthropometry Resource (CAESAR), Final Report, Volume I: Summary*. Sytronics Inc, Dayton Ohio.
- Rodriguez-Florez, N., JL. Bruse, A. Borghi, H. Vercruyse, J. Ong, G. James, X. Pennec, DJ. Dunaway, NO. Jeelani, and S. Schievano. 2017. "Statistical Shape Modelling to Aid Surgical Planning: associations between Surgical Parameters and Head Shapes following Spring-Assisted Cranioplasty." *International Journal of Computer Assisted Radiology and Surgery* 12 (10): 1739–1749. doi:[10.1007/s11548-017-1614-5](https://doi.org/10.1007/s11548-017-1614-5).
- Rousseeuw, PJ. 1987. "Silhouettes: A Graphical Aid to the Interpretation and Validation of Cluster Analysis." *Journal of Computational and Applied Mathematics* 20: 53–65. doi:[10.1016/0377-0427\(87\)90125-7](https://doi.org/10.1016/0377-0427(87)90125-7).
- Seidl, A., R. Trieb, and HJ. Wirsching. 2009. SizeGERMANY—the New German Anthropometric Survey conceptual design, implementation and results. Proceedings of 17th World Congress on Ergonomics.
- Sena, K., and S. Piyasin. 2008. "Determination of Average Contour of Thais Skulls for Design of Implants." *American Journal of Engineering and Applied Sciences* 1 (3): 168–173. doi:[10.3844/ajeassp.2008.168.173](https://doi.org/10.3844/ajeassp.2008.168.173).
- Seo, H., Jl. Kim, and H. Kim. 2020. "Development of Korean Head Forms for Respirator Performance Testing." *Safety and Health at Work* 11 (1): 71–79. doi:[10.1016/j.shaw.2019.12.008](https://doi.org/10.1016/j.shaw.2019.12.008).
- Skals, S., T. Ellena, A. Subic, H. Mustafa, and TY. Pang. 2016. "Improving Fit of Bicycle Helmet Liners Using 3D Anthropometric Data." *International Journal of Industrial Ergonomics* 55: 86–95. doi:[10.1016/j.ergon.2016.08.009](https://doi.org/10.1016/j.ergon.2016.08.009).
- Taylor, NA., HH. Fullagar, BJ. Mott, JA. Sampson, and H. Groeller. 2015. "Employment Standards for Australian Urban Firefighters: Part 1: The Essential, Physically Demanding Tasks." *Journal of Occupational and Environmental Medicine* 57 (10): 1063–1071. doi:[10.1097/JOM.0000000000000525](https://doi.org/10.1097/JOM.0000000000000525).
- Verwulgen, S., D. Lacko, J. Vleugels, K. Vaes, F. Danckaers, G. De Bruyne, and T. Huysmans. 2018. "A New Data Structure and Workflow for Using 3D Anthropometry in the Design of Wearable Products." *International Journal of Industrial Ergonomics* 64: 108–117. doi:[10.1016/j.ergon.2018.01.002](https://doi.org/10.1016/j.ergon.2018.01.002).
- Wang, J., J C. Thornton, S. Kolesnik, and R N. Pierson. 2000. "Anthropometry in Body Composition: An Overview." *Annals of the New York Academy of Sciences* 904 (1): 317–326. doi:[10.1111/j.1749-6632.2000.tb06474.x](https://doi.org/10.1111/j.1749-6632.2000.tb06474.x).
- Wang, M-JJ., EM-y Wang, and Y-C. Lin. 2002. "The Anthropometric Database for Children and Young Adults in Taiwan." *Applied Ergonomics* 33 (6): 583–585. doi:[10.1016/s0003-6870\(02\)00032-7](https://doi.org/10.1016/s0003-6870(02)00032-7).
- Weisberg, S. 2005. *Applied Linear Regression*. Vol. 528. New Jersey, USA: John Wiley & Sons.
- Xi, W., W. Zongqian, and L. Qiao. 2022. "Extraction of Feature Points for Non-Uniform Rational B-Splines (NURBS)-Based Modeling of Human Legs." *Journal of Donghua University* 39 (4): 479–484.
- Xie, S., N. Li, and Z. Lv. 2010. Human Head Modeling Using NURBS Method. In *Advances in Neural Network Research and Applications*. 479–484. New York, USA: Springer Nature.
- Zhang, B., and J. Molenbroek. 2004. "Representation of a Human Head with bi-Cubic B-Splines Technique Based on the Laser Scanning Technique in 3D Surface Anthropometry." *Applied Ergonomics* 35 (5): 459–465. doi:[10.1016/j.apergo.2004.03.012](https://doi.org/10.1016/j.apergo.2004.03.012).
- Zhang, J., H. Iftikhar, P. Shah, and Y. Luximon. 2022a. "Age and Sex Factors Integrated 3D Statistical Models of Adults' Heads." *International Journal of Industrial Ergonomics* 90: 103321. doi:[10.1016/j.ergon.2022.103321](https://doi.org/10.1016/j.ergon.2022.103321).
- Zhang, J., K. Zhou, Y. Luximon, P. Li, and H. Iftikhar. 2022c. "3D-Guided Facial Shape Clustering and Analysis." *Multimedia Tools and Applications* 81 (6): 8785–8806. doi:[10.1007/s11042-022-12190-x](https://doi.org/10.1007/s11042-022-12190-x).
- Zhang, J., Y. Luximon, P. Shah, K. Zhou, and P. Li. 2022b. "Customize My Helmet: A Novel Algorithmic Approach Based on 3D Head Prediction." *Computer-Aided Design* 150: 103271. doi:[10.1016/j.cad.2022.103271](https://doi.org/10.1016/j.cad.2022.103271).
- Zhuang, Z., and B. Bradtmiller. 2005. "Head-and-Face Anthropometric Survey of US Respirator Users." *Journal of Occupational and Environmental Hygiene* 2 (11): 567–576. doi:[10.1080/15459620500324727](https://doi.org/10.1080/15459620500324727).
- Zhuang, Z., C. Shu, P. Xi, M. Bergman, and M. Joseph. 2013. "Head-and-Face Shape Variations of US Civilian Workers." *Applied Ergonomics* 44 (5): 775–784. doi:[10.1016/j.apergo.2013.01.008](https://doi.org/10.1016/j.apergo.2013.01.008).
- Zhuang, Z., D. Landsittel, S. Benson, R. Roberge, and R. Shaffer. 2010. "Facial Anthropometric Differences among Gender, Ethnicity, and Age Groups." *The Annals of Occupational Hygiene* 54 (4): 391–402. doi:[10.1093/annhyg/meq007](https://doi.org/10.1093/annhyg/meq007).
- Zhuang, Z., S. Benson, and D. Viscusi. 2010. "Digital 3-D Headforms with Facial Features Representative of the Current US Workforce." *Ergonomics* 53 (5): 661–671. doi:[10.1080/00140130903581656](https://doi.org/10.1080/00140130903581656).